THERMIONIC EMISSION – A KEY TO UNDERSTANDING HIGH TEMPERATURE ELECTROSTATIC PRECIPITATION

Ulrich Riebel*, Patrick Bürger, Ahmad Al-Issa, Jan Stepputat
Lehrstuhl Mechanische Verfahrenstechnik
Brandenburgische Technische Universität Cottbus-Senftenberg
03013 Cottbus, Germany

*corresponding author: Ulrich.Riebel@b-tu.de

Please Note: Large parts of this conference paper are already part of a paper which is being prepared for a regular journal publication. Therefore this paper will not be available for publication in Springer LNEE.

ABSTRACT. For high temperature corona discharges, the range of operation becomes narrower with increasing temperature, as the decrease of sparking voltage is much more pronounced compared to the drop of corona onset voltage. However, at high temperatures the thermionic emission of electrons allows the operation of ESPs at voltages below corona onset, which will avoid sparking.

In order to provide a better understanding and to allow a proper dimensioning of high-temperature ESPs operated in the sub-onset range, thermionic emission from real, oxidized metal surfaces was studied in a precise laboratory experiment covering the temperature range between 500 °C and 800 °C. The main findings are (i) A Richardson constant which is far (20- to 40-fold) lower compared to the theoretical value. (ii) Very low values of the work function, which are around 3 eV only. (iii) A very pronounced Schottky effect, due to surface roughening and local field enhancement.

Altogether, the operation of ESPs in the sub-onset mode opens a number of interesting perspectives: (i) Thermionic emission allows stable ESP operation in the sub-onset mode for a wide range of temperature, starting at about 700 °C. (ii) Particle charging by non-thermal (hot) free electrons is extremely fast and highly efficient, providing high charge levels already with a current density in the range of µA/m and short residence time. (iii) Therefore, ESPs operated with sub-onset thermionic emission have low power requirements and offer high energy efficiency.

KEYWORDS: Electrostatic precipitation, Thermionic emission, Free electrons, Work function, Schottky effect, Richardson constant, Field enhancement factor.

Acknowledgements: Thanks are due to Mr. Uwe Zernsdorf and Mr. Florian Schmaler (machine shop) and to the students (Patrick Kuhnert, Aness Sayah, Prasad Shinde) who were involved into the installation and the measurements.

1 Introduction

After the removal of dusts and aerosols, the heat content of flue gases can be used much easier in heat exchangers and regenerators. Therefore, high-temperature (HT) gas cleaning is an important tool to reach a higher efficiency of energy use in a multitude of industrial processes. But still, there is very little industrial experience with ESP operation at temperatures going beyond about 450 °C [Parker 1997].

The present research is motivated by observations showing that HT-ESPs can achieve good or even excellent separation efficiency when being operated at voltages which are still below corona onset [Bürger 2022-2]. We may call this mode of operation the sub-onset mode of operation (SOMOO). The physics of ESPs in the SOMOO is quite complicated and not yet fully understood. In the SOMOO, the dominating process of current generation in the ESP is thermionic emission (TE).

In all of the references on HT-ESPs which we could find so far, TE is understood as the emission of free electrons. However, this restriction of view is not at all axiomatic. As a matter of fact, technical HT-ESPs are quite dirty systems. Due to oxidation, corrosion and particle deposition, metallic surfaces are an exception. Numerous hints from other fields of research indicate that the conditions in HT-ESPs should also allow for the emission of anions and cations from solid surfaces. But in the present research, compounds which are known to emit cations and anions, notably alkai metal salts, were absent and there were not hints on the TE of positive charge carriers.

From the practical side, it appears that the electrode currents generated by TE can have an influence on the ESP performance from about 600 °C upwards. From about 700°C on, thermionic currents appear to be sufficiently high to allow an ESP operation in the SOMOO. This is especially attractive, as the SOMOO features a low consumption of energy and avoids sparking even with negative corona polarity. This opens a perspective to design HT-ESPs which are suitable for operation at near-ambient pressure, while using free electrons as a means to reach the most efficient charging of particles [Bürger 2022-2].

2 State of Knowledge

In view of technical coronas applied in aerosol chargers and electrostatic precipitators for gas cleaning, the most important information on a corona discharge is the CVC. In typical applications with low and moderate temperatures of operation, the CVC starts with the corona onset voltage and ends with the sparkover voltage. In cases of HT-ESPs with thermionic emission however, significant currents, particle charging and particle separation are found below corona onset already.

The present paper will focus on the sub-onset range of the CVC, which has been widely neglected so far. In a first step, we will discuss experimental results on HT CVCs or HT ESPs which show some influence from thermionic emission. This review will also include results on the charging of aerosols

by thermionic emission. In a second step, we try to provide a systematic overview on the physical background of thermionic emission.

2.1 Experimental Studies on High Temperature Coronas

Starting from the late 1950es, researchers have provided a large body of experimental data on corona discharges at elevated temperatures. However, awareness for the effects of thermionic emission in ESPs can be traced back only to the late 1980es.

Rinard et al (1987) demonstrated dust removal from a combustion gas on a semi-technical scale (tube diameter $d_t = 305\ mm$) with positive and negative corona operating at 1016 K and 1189 K and 6.4 bar. The collection efficiency responded to variations of the average field without significant influence from temperature. With dust and high temperatures, a strong increase of current uptake is observed, which is ascribed to thermionic emission of electrons from the dust.

Weber et al. (1993) report on a high-temperature-high-pressure plate-wire-ESP on a semi-industrial scale allowing operation at up to 1273 K and 20 bars. Hot flue gases are produced by combustion of methane or coal dust. At temperatures above 973 K to 1023 K, the negative corona onset voltage appears to vanish due to thermionic emission from the electrodes and possibly, also due to leak currents across the high voltage (HV) insulations. Good precipitation results are reported with electrodes which do not produce a corona.

Gu et al. (2012) present a two-stage tubular ESP with rather small tube diameter (41 mm) featuring a highly emissive rare earth-tungsten (RE-W) electrode. The effect of thermionic emission on CVCs is shown for temperatures between 1073 K and 1473 K. Using extremely high current densities, fly ash can be separated at temperatures up to 1273 K. Even though sub-onset mode and corona mode cannot be distinguished clearly from the CVCs, the selection of the RE material appears to influence precipitation efficiency significantly. However, the conditions of operation are not fully traceable. Xu et al. (2022) present further results with the RE-W cathodes for temperatures going up to 1373 K.

Altogether, serious attempts to bridge the gap between experimental observations and theoretical understanding are still scarce, and the validity of theoretical knowledge for the description of HT-ESPs has not yet been challenged. Therefore, in the next section, we are going to discuss high temperature effects with specific attention to thermionic emission.

2.2 Thermionic Emission

In a rather broad definition which we adopt here, thermionic emission (TE) refers to the emission of mobile charge carriers into a gas phase or into a vacuum. The process of TE can be observed with various species of charge carriers and requires a specific amount of activation energy which is called the work function W.

Emission of electrons from metal surfaces. At high temperature, free electrons can be emitted from metal surfaces by the mechanism of thermionic emission (TE). In case of TE, the energy for an electron to leave the electrode surface is provided by the thermal energy. The current density of

electrons emitted from a metal surface was first determined experimentally by Richardson (1929). In the presence of an external E-field, the effective work function for electron emission is lowered by the Schottky effect. Quantitatively, the current density j from TE [Jenkins 1969], [Raizer 1991] is described by:

$$j = A_R T^2 \exp\left(-\frac{W_e}{k_B T}\right) \exp\left(\frac{\Delta W}{k_B T}\right) = A_R T^2 \exp\left(-\frac{(W_e - \Delta W)}{k_B T}\right) \qquad \text{Eq. (7)}$$

where W_e is the work function of the electron, and $k_B T$ the thermal energy. The Richardson constant A_R ($A_R = 1.2 \cdot 10^6\ A/(m^2\ K^2)$) can be derived from fundamental physical constants, but experimental values may differ significantly. Further, ΔW describes the Schottky effect, which consists in a reduction of the effective work function of the electron $W_{e,eff}$ due to an external electric field at the emitting surface:

$$W_{e,eff} = W_e - \Delta W \qquad \text{Eq. (8)}$$

whereby

$$\Delta W = \sqrt{\frac{e^3 E}{4\pi\varepsilon_0}} \qquad \text{Eq. (9)}$$

ΔW reaches a value of 0.12 eV @ 100 kV/cm ($10^7\ V/m$) , which is still quite small compared to the work function of most materials, but comparable to $k_B T$ at 1400 K ($k_B \cdot 1400\ K = 1.93 \cdot 10^{-20}\ J = 0.121\ eV$). Hence the Schottky effect will be most significant for TE from thin corona wires with very high values of the corona onset field E_0.

W_e values of different materials typically are given for smooth clean surfaces under vacuum conditions. For many metals like copper, nickel, iron, stainless steel and the noble metals, W_e is in a range of 4.5 to 6.5 eV [Raizer 1991], [Wilson 1966].

Going into detail, W_e is slightly dependent on temperature and very generally, a decrease of W_e with increasing temperature is found [Durakievicz 2001]. [Wilson 1966] has measured W_e values for stainless steel decreasing from 4.34 eV @ 1085 K down to 4.22 eV @ 1395 K. The Wilson measurement corresponds to a temperature coefficient of $38.7 \cdot 10^{-5}\ eV/K$, while theoretical and experimental temperature coefficients compiled by Durakievicz (2001) are in a range of $5\ to\ 15.5 \cdot 10^{-5}\ eV/K$ for elemental Fe.

Darcy & Surplice (1973) report W_e values of 4.7 to 5.6 eV for oxidized stainless steel at ambient temperature.

Emission of electrons from metal oxides. For 18 different metal oxides, mostly transition metals, Rietwijk et al. (2019) state a significant decrease of W_e when the oxide layers produced by deposition from the vapour phase in vacuum are exposed to air for several hours. The range of W_e values, all measured at ambient temperature, goes from 4.9 eV (Cr_2O_3) through 4.5 eV (Ce_2O_3, Fe_2O_3) to 4.3 eV ($Ti\ O_2$).

In analogy to the emission of free electrons from metal surfaces, other types of charge carriers can be emitted from various surfaces.

Emission of negative gas ions. The surfaces of many materials which are active as oxidation catalysts are known to be covered by adsorbed oxygen, whereby different oxygen species are assumed to be in equilibrium:

$$O_{2\,(g)} \Leftrightarrow O_{2(ads)} \overset{e^-}{\Leftrightarrow} O_2^- \overset{e^-}{\Leftrightarrow} O_2^{2-} \Leftrightarrow 2\,O^- \overset{2\,e^-}{\Longleftrightarrow} 2\,O^{2-} \qquad (10)$$

This appears to be the case for noble metals and also for different metal oxides, including Cr_2O_3 and Fe_2O_3 [Christensen 2016]. Experimental results on catalytic soot oxidation give proof that some of these species, notably O^{2-}, are mobile and may diffuse through layers of inert (ash) particles. This effect is known as catalytic spillover or "remote oxidation" [Yamazaki 2014]. For the specific case of catalytic soot oxidation with layers of soot and Pt catalyst separated by an air gap, Zeng & Weber (2012) have shown that the activated oxygen is mainly transported through the gas phase, having a maximum life of 65 ms.

A group of interesting materials are the oxygen ion conducting materials [Skinner & Kilner (2003)]. A well-known material out of this group is Yttrium-modified ZrO_2 ceramics (YSZ). Nishioka et al. (2003) quantified that O^- and free electrons are emitted from YSZ in a ratio which is near 1:1 and with similar energy of activation. In the lower temperature range (450 – 620 °C), the work function was higher (around 220 kJ/mol = 2.28 eV) compared to the range of higher temperatures (620 °C to 750 °C) with a work function value of around 75 kJ/mol (0.78 eV).

Alkali Cation Emission. The actual set-up basically does not allow to distinguish between the emission of anions or free electrons from the cathode and the emission of cations from the anode. Therefore, the emission of cations must be considered as a further mechanism leading to sub-onset currents. In numerous references, the thermal desorption of alkali metal cations is discussed, owing to the comparatively low activation energy of this process.

The emission of alkali ions from rhodium and stainless steel surfaces into air was studied by Hagström et al. (2000). The alkali ions were provided as an alkali salt aerosol. The activation energies for desorption from stainless steel were 2.88 eV (1010 K to 1390 K) for Na^+ and 3.63 eV (950 – 1110 K) or 1.75 eV (1110 – 1450 K) for K^+, depending on the temperature range. Lower desorption energies (starting with 0.99 eV) were found for alkali ions emitted from impurities contained in the steel itself. For K^+ desorption from a Pt wire into air, an activation energy of 2.49 eV was found. Generally, the activation energy for the cation does not depend on the anion, but it is influenced by the surface coverage.

The desorption of K and K^+ from K-impregnated $Al_2\,O_3$ and K-impregnated or K-substituted $Sr\,Ti\,O_3$ into air was studied by Ura et al. (2011). The activation energy of the two K species was found to be in a range from 1.8 to 2.3 eV, while the work function of electrons was between 3,5 and 5.1 eV.

3 Experimental Set-up

Experimental Challenges. Thermionic currents are on a rather low level. Meanwhile, the measurement of such low currents in the presence of high voltages and high temperatures poses a number of severe challenges.

In the first place, the ceramic insulation materials used as holders for the corona wires are not perfect. According to data provided by Wilson (1981), MgO and Al_2O_3 are the ceramic materials offering the best electrical insulation at high temperature. But already at temperatures of around 600 °C, the resistivity of Al_2O_3 falls below $10^{12}\ \Omega cm$, and with voltages of several 10 kV, current losses through typical laboratory insulator constructions are approaching the range of 1 µA. Second, the problem of imperfect insulation also applies to the cables connecting the HV supply to the working electrode WE (As we avoid corona operation, we also avoid the notion of corona electrode). Leak currents are typically limited either by the injection work function or by space charge effects within the insulation layer [Lampert 1956, Serdyuk & Gubanski 2005]. In our set-up, we found cable leak currents in the µA range. At ambient temperature, these problems can be avoided when the corona current is measured at the precipitation electrode PE as I_{PE}. At high temperature however, this does not work as the PE is surrounded by an outer housing. Thermionic currents emitted from the housing and the electric heating coils can be collected on the PE and generate a strong bias on I_{PE}.

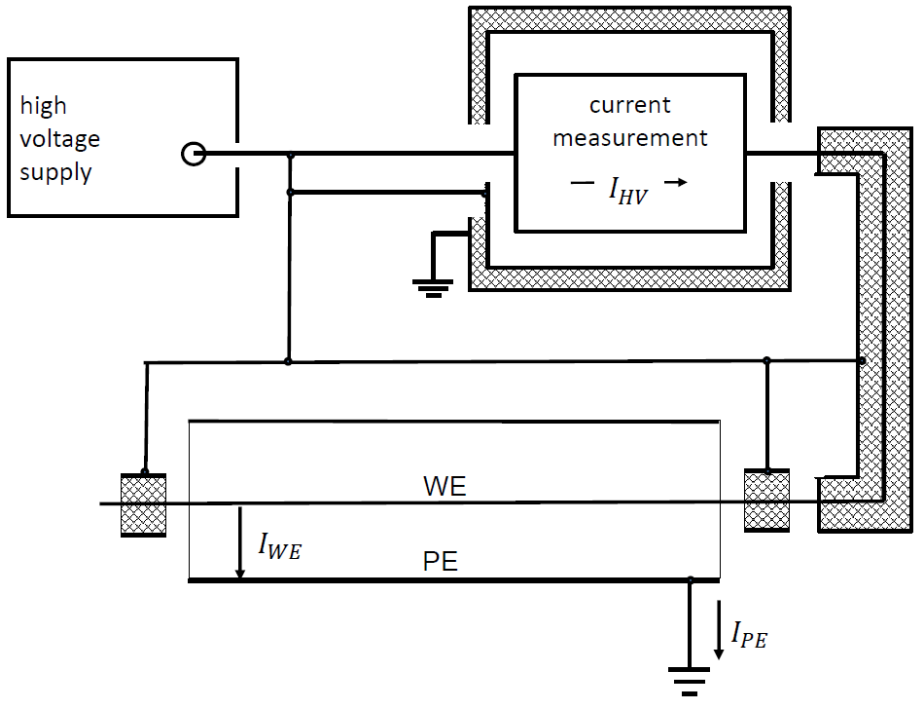

Fig. 1: *Sketch of the electric circuit used for the measurement of the thermionic currents.*

An additional, but minor problem of electrical insulation results from thermoelectric and electrochemical bias currents, which are originating mainly from the ceramic wire holders. The insulation material IM forming a bridge between two metal electrodes (here: WE and PE) may act both as a conductor or as an electrolyte.

Experimental Set-up. As a result, the best choice is the direct measurement of I_{HV} , which is the current on the high voltage side, Fig. 1. In a special arrangement, the central high voltage conductor (connecting the WE to the power supply and serving for the measurement of U_{HV}) is surrounded by

a concentric high voltage guard which is supplied with exactly the same potential. Sections of the central lead which cannot be shielded due to a difficult geometry are protected with supplementary silicon rubber hoses. In this way, current losses are reduced to a minimum.

Fig. 2 shows the construction of the ceramic WE holder. The WE holders comprise, from inside to outside:

(i) A central conductor for the HV supply to the WE, on which the current is measured, on one side. On the other side, there is only a wire tensioning mechanism with a spring.
(ii) An Al_2O_3 tube (20 mm outer diam.) for electrical insulation.
(iii) A stainless steel tube (23 mm inner diam.) with end caps acting as mechanical support for the inner Al_2O_3 tube. For shielding current losses across ceramic tube (ii), this metal tube is connected to the same potential as the corona wire.
(iv) An outer Al_2O_3 tube limiting current losses to the grounded PE. This ceramic tube is fixed in the end plate of the tube using a wedge packing.

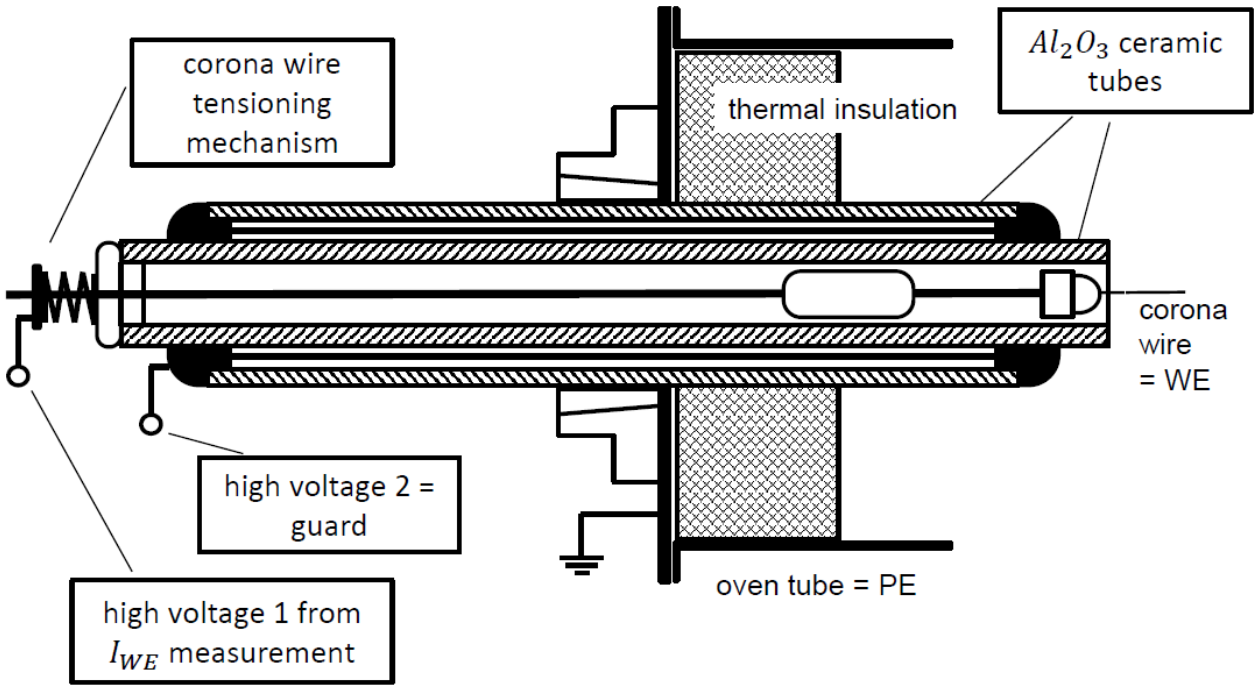

Fig. 2: *Corona wire holder and tensioning system mounted to the end of the oven tube. The guard voltage is equal to the corona wire voltage and reduces bias currents by several orders of magnitude.*

Central part of the experimental set-up is the tube-shaped precipitation electrode PE (inner diameter 78 mm, length 1200 mm) with the working electrode WE in its centre. On both ends, the precipitation tube is closed the wire holders corresponding to Fig. 2. The net length of the WE (between the ends of the inner ceramic tubes) amounts to 860 mm at ambient temperature.

In order to avoid the accumulation of NOx generated in the corona discharge, a small flow of dried air (5 ltr./min, dew point – 26.9 °C) is introduced through one of the inner ceramic tubes. Without this air flow, some reduction of corona current with time would be observed.

The average temperature of the tube was determined from three thermocouples placed inside the tube the centre and at the ends of the wire.

4 Results and Discussion

4.1 Experimental Current-Voltage-Characteristics

Measurements of sub-onset currents have been made and evaluated in a wide range, covering temperatures between about 773 K (500 °C) and 1073 K (800 °C). Measurements at lower temperatures have been made in several occasions, but the thermionic currents were below the limit of resolution.

In detail, the measurement procedure was as follows: The measurements shown here were executed with a new piece of wire made from heat resistant stainless steel 1.4820. Before the start of the experiments, the wire was burnt-in at 1002 K for about 5 hours. The tube from stainless steel 1.4404 had been in use previously for about 100 hours at different temperatures up to 1073 K. Between different experimental runs, the inner tube surface was cleaned using a wet polyester cloth.

The original experimental data are presented as current-voltage characteristics (CVCs). The polarity of the current values displayed in the diagrams always corresponds to the corona polarity. The current readings at 0 kV were always positive and are displayed together with the currents measured for TE from the tube (or, at positive WE polarity).

Displaying the current on a logarithmic scale and the operation voltage U as $\sqrt{U}$, we obtain a Schottky diagram. In this mode of presentation, the Schottky effect should lead to a linear slope in the regime of thermionic emission. Below about 1 kV of operation voltage, currents deviate from the Schottky behaviour, because a part of the electrons emitted into the gas re-diffuses back to the emitting electrode. By linear extrapolation from the range of higher voltages to $U = 0$, the Schottky diagrams allow to eliminate graphically both back-diffusion and the Schottky effect.

When approaching to the corona onset voltage U_0, we also find deviations from Schottky law, leading to a somewhat diffuse transition between the ranges of TE and of corona discharge. These deviations are explained by the fact that slightly below the onset voltage, the E-field near the surface of a corona electrode is already above the ionization limit. This in turn leads to some multiplication of free electrons originating from TE.

Figs. 3 and 4 show Schottky plots based on the original current measurements. We see that the thermionic currents increase from less than a nA to about 30 µA, depending on temperature and voltage. As the effective resolution of the current measurements is not too much below 0.1 nA, the measurements at 829 K are not free from bias. This will become evident during the more detailed evaluation.

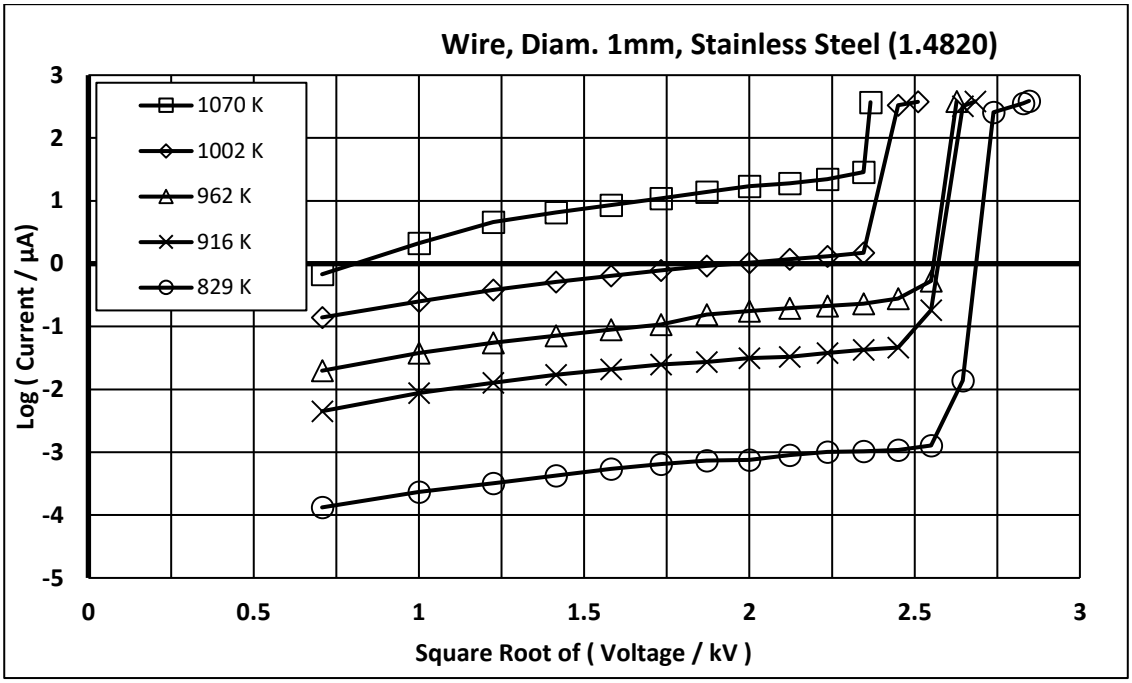

Fig. 3: *Original measurements of current-voltage-characteristics showing a Schottky plot of the sub-onset range for temperatures between 829 K and 1070 K. For the wire, thermionic emission is measured at negative polarity. At zero voltage, the currents are positive and hence will be shown together with the emission currents from the tube. The corona onset is found on the right-hand side. The current is limited to a maximum of 0.5 mA.*

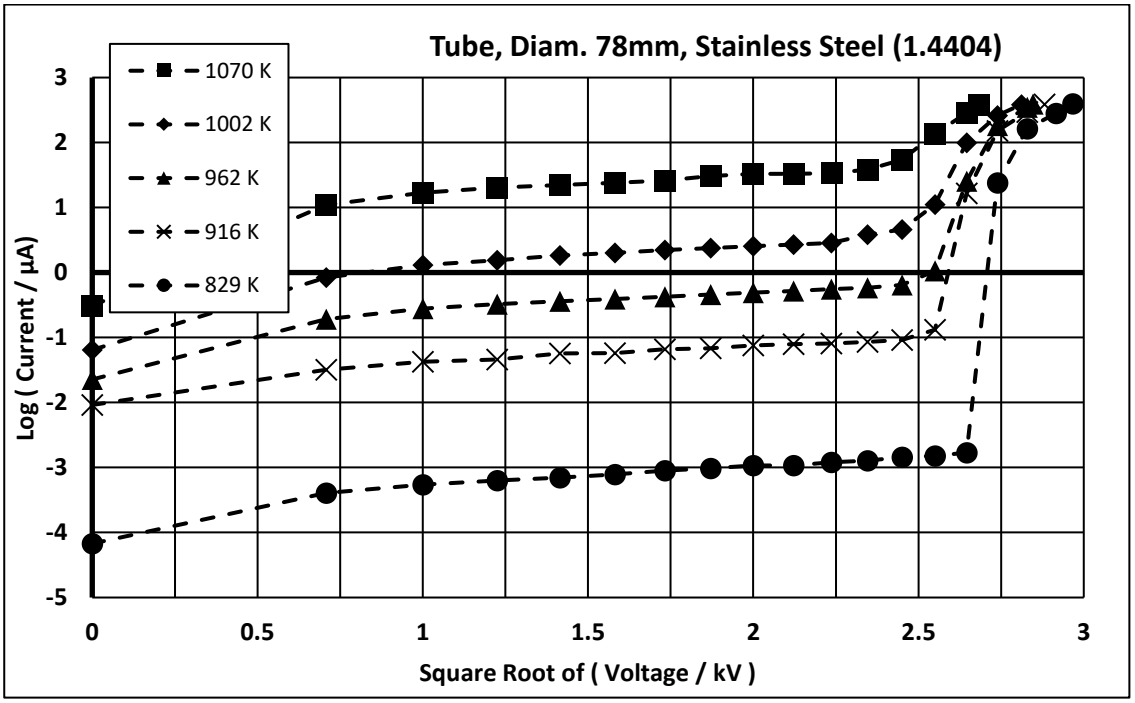

Fig. 4: *Original measurements of current-voltage-characteristics showing the sub-onset range for temperatures between 829 K and 1070 K. For the tube, thermionic emission is measured at positive polarity. The corona onset is found on the right-hand side. The current is limited to a maximum of 0.5 mA.*

5 Evaluation and Discussion

As discussed already in the theoretical part, the measurements described here do not allow any distinction with respect to the species being emitted and producing the current. On the other hand, the authors had studied charge carrier mobilities, aerosol particle charging and precipitation already before, using a rather similar set-up built from similar materials [Bürger 2022-1, Bürger 2022-2]. These measurements provide us with strong arguments that TE is dominated, in the present case, by free electrons:

- measurements of the charge carrier mobility have shown a linear increase of positive charge mobility for most of the temperature range (up to 1023 K), while negative charge carrier mobility deviated from a linear increase at temperatures above about 473 K. At higher temperatures, negative charge carrier mobility reaches values which are far beyond the mobilities of the smallest ions.

- measurements of aerosol particle polarity have shown purely negative charging in case of negative WE (wire or rod) polarity. This excludes any significant emission of positive ions from the PE. In contrast, purely negative aerosol polarity if found when the WE is operated in the sub onset range. This proves that in the sub onset regime with positive polarity, only negative charge carriers do exist which are emitted from the grounded PE.

- With negative WE (wire or rod) polarity in general, or with positive WE (rod) polaritiy in the SOMOO regime, uncommonly high precipitation efficiencies were found and uncommonly high levels of negative particle charge were measured. This proves the existence of free electrons with a high electron temperature, however without excluding the existence of negative gas ions.

Based on this knowledge, our further evaluation assumes that only negative charge carriers with a uniform work function W_e are emitted in the present experiment. This assumption is compatible with the emission of free electrons, or with a combined emission of free electrons and negative oxygen species as discussed in section 2.2.

The evaluation of the TE measurements involves the determination of a number of independent parameters, notably the effective work function W_{eff} (as a function of voltage) or the work function W_e, and the experimental Richardson constant A_{exp}. Further, a field enhancement factor will be introduced in order to obtain a more realistic description of the Schottky effect.

5.1 Effective Work Function Using the Theoretical Richardson Constant.

A simple approach for determining the effective work function W_{eff} is based on the assumption that the Richardson constant is known and corresponds to the theoretical value A_R. With A_R , the emissive area and the temperature known, each single current reading can be used to calculate the corresponding value of W_{eff}. Equal or equivalent procedures are found in several of the references. However, there are some points of criticism:

- Experimental values A_{exp} can differ significantly from the theoretical value A_R.
- The microscopic surface area might be larger than the apparent surface.
- A significant fraction of the surface might be inactive due to surface roughness.

- The surface might be chemically inhomogeneous, so that TE is dominated by a small fraction of the surface having the lowest W_e.
- The emitting area might be ill-defined. In our case, this applies to the emissive areas of the wire and of the precipitation tube, which are biased by edge effects from the wire holders.

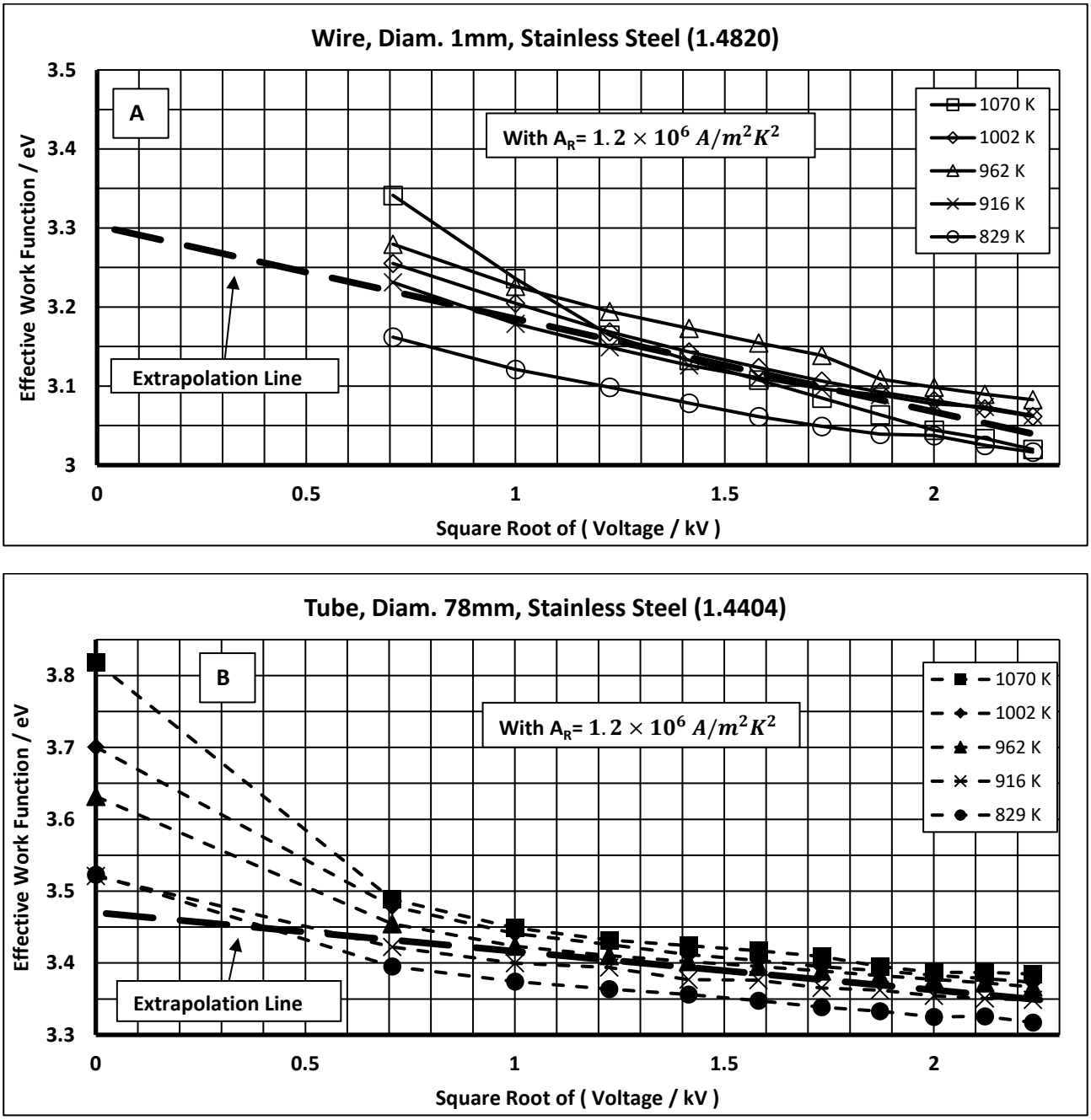

Fig. 5: *Effective work function W_{eff} as determined from the original current measurements, assuming the theoretical value of the Richardson constant to be valid. Besides the single measurement points for the different combination of temperature and voltage, a temperature-averaged trend is calculated for the range from* 1 *to* $2.25\ \sqrt{kV}$ *and extrapolated to* $0\ \sqrt{kV}$. ***(A)****, above: W_{eff} for emission from the wire at negative operation voltage. The extrapolated trendline indicates a W_e of* $3.30\ eV$ *for the wire.* ***(B)****, below: W_{eff} for emission from the tube at positive operation voltage. The extrapolated trendline indicates a W_e of* $3.47\ eV$ *for the tube.*

In spite of the criticism discussed above, we have applied this over-simplified approach of evaluation in order to understand the type and magnitude of errors arising from this. **Fig. 5** shows W_{eff} for the wire and the tube, respectively. The curves are found within a band having a width of about $\pm 0.1\ eV$ in the linear range extending between $1/\sqrt{kV}$ and $2.25/\sqrt{kV}$. Deviating from theoretical expectation and independent experimental results, we can observe a trend of increasing W_{eff} values with increasing temperature. This is most clearly visible in case of the tube, **Fig. 5b**. Also deviating from theory, the slope of W_{eff} falling off with increasing $\sqrt{U}$ is much higher compared to the theoretical expectation. As a consequence of these deviations, we shall try to determine experimental values for the Richardson constant, and we shall have to develop a modification of the Schottky theory.

5.2 Empirical Richardson Constants

An empirical Richardson constant A_{exp} can be determined directly from two current measurements at different temperature, but equal voltage. For this, we use the Richardson equation (Eq. (7)) combined with the assumption that W_{eff} does not depend on temperature:

$$\frac{W_{eff}}{k_B} = T_1\ ln\left(\frac{A_{exp}\ T_1^2}{j_1}\right) = T_2\ ln\left(\frac{A_{exp}\ T_2^2}{j_2}\right) \tag{11}$$

This leads to

$$ln\left(\frac{A_{exp}\ T_2^2}{j_2}\right)^{\frac{T_2}{T_1}} = ln\left(\frac{A_{exp}\ T_1^2}{j_1}\right) \tag{12}$$

After some rearrangement, we finally obtain

$$A_{exp} = \left[\frac{\frac{T_1^2}{j_1}}{\left(\frac{T_2^2}{j_2}\right)^{\frac{T_2}{T_1}}}\right]^{\frac{1}{\frac{T_2}{T_1}-1}} \tag{13}$$

Negative Voltage [kV]	Temperatures T_1 & T_2 $[K]$			
	829 & 916	**829 & 962**	**829 & 1002**	**829 & 1070**
1	5.4E+02	1.3E+02	4.5E+03	4.7E+03
1.5	1.4E+03	2.8E+02	1.1E+04	5.0E+04
2	2.0E+03	3.1E+02	1.6E+04	8.8E+04
2.5	1.7E+03	3.5E+02	1.9E+04	1.3E+05
3	2.0E+03	4.8E+02	2.6E+04	2.1E+05
3.5	1.6E+03	2.8E+03	3.4E+04	3.7E+05
4	5.7E+03	5.9E+03	6.2E+04	8.6E+05
4.5	1.8E+03	4.3E+03	5.5E+04	8.0E+05

Positive Voltage [kV]	Temperatures T_1 & T_2 $[K]$			
	829 & 916	**829 & 962**	**829 & 1002**	**829 & 1070**
1	3.9E+04	1.6E+04	1.4E+04	3.3E+04
1.5	2.2E+04	2.0E+04	1.9E+04	4.4E+04
2	7.6E+04	2.2E+04	2.9E+04	4.5E+04
2.5	2.8E+04	1.9E+04	2.9E+04	4.3E+04
3	3.4E+04	1.5E+04	2.8E+04	4.0E+04
3.5	2.4E+04	1.6E+04	2.8E+04	6.0E+04
4	2.4E+04	1.3E+04	2.5E+04	6.1E+04
4.5	4.4E+04	2.1E+04	3.5E+04	6.3E+04

Table 1: *Results for the experimental Richardson constant A_{exp} (in A/m^2K^2) calculated with Eq. (13) for different voltages of operation and using different pairs of temperature.*

An overview of A_{exp} values obtained on basis of Eq. (13) is shown in **Table 1**. The values include all possible temperature combinations and fully cover the voltage range in which the Schottky ΔW is valid. Obviously, the current data for TE from the tube are more consistent and produce less scatter in the A_{exp} results. Using all the values included in the tables, we have calculated averaged values of A_{exp} for the wire and for the tube separately, amounting to $A_{exp} = 6.8 \times 10^4\ A/m^2K^2$ for the wire and to $A_{exp} = 3.1 \times 10^4\ A/m^2K^2$ for the tube, respectively. This is about a factor of 20 to 40 lower compared to the theoretical value.

5.4 Effective Work Function and Work Function Calculated with Empirical Richardson Constants

When the procedure of section 5.1 is repeated using the A_{exp} values from section 5.3, we obtain a corrected presentation of the W_{eff} values which is shown as **Fig. 6**. With $A_{exp} \ll A_R$, identical TE currents are now explained by significantly smaller values of W_{eff} and W_e, respectively. From Eq. (7) we find that a deviation of 0.1 eV in W_e is compensated by a change of A_{exp} by a factor of 3.63 @ 900 K. For the tube and for the wire we now find values of $W_{e,tube} = 3.17\ eV$ and of $W_{e,wire} = 3.11\ eV$, respectively. Moreover, the trend of W_{eff} shifting systematically with temperature is eliminated more or less completely, as this was an assumption included in the derivation of Eq. (13). Meanwhile, the W_{eff} data for TE from the wire still show more scatter around the trend line, which must be attributed to a lower quality of these data.

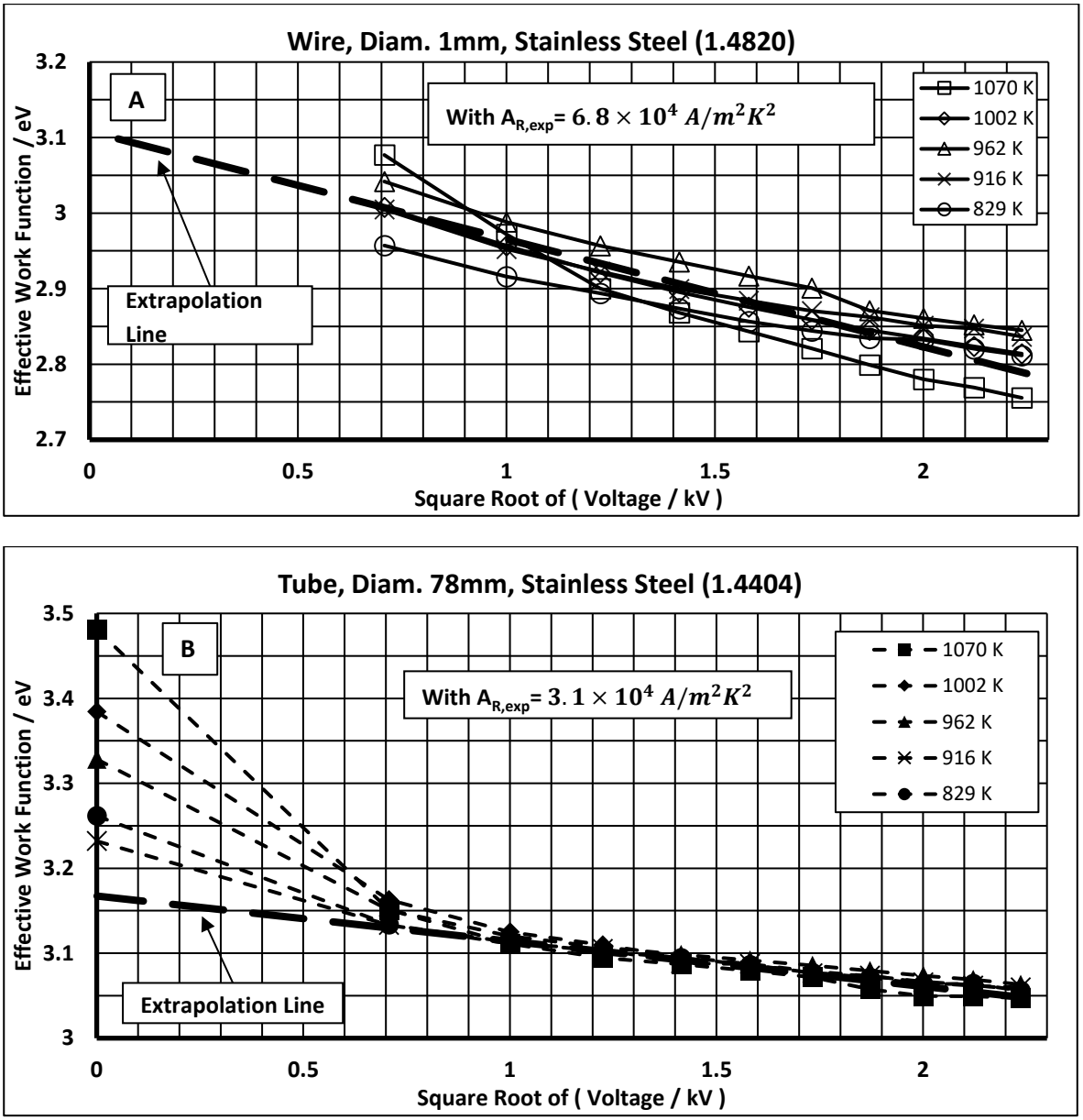

Figure 6: *Schottky diagrams for W_{eff}, calculated with the empirical values of the Richardson constant A_{exp} as indicated in the diagrams. (**A**), above: W_{eff} for emission from the wire at negative operation voltage. The extrapolation indicates a W_e of* 3.11 *eV for the wire. (**B**), below: W_{eff} for emission from the tube at positive operation voltage. The extrapolation indicates a W_e of* 3.17 *eV for the tube.*

5.5 Effective Work Function and Work Function from Differential Calculations

As the determination of the A_{exp}values is very sensitive to experimental errors, we may seek an alternative path for a correct determination of W_{eff} and W_e. Further we know from the references discussed in section 2.2, that the assumption of a temperature independent W_{eff} or W_e is most questionable. In fact, our data cover a temperature range of nearly 250 K. With temperature coefficients reported to be between $5\ and\ 38.7 \cdot 10^{-5}\ eV/K$, these values might decrease by $0.0125\ to\ 0.1\ eV$ within our temperature range.

Most of the potential errors are avoided, when W_{eff} is determined from the ratio of TE current densities measured at two different temperatures T_1 and T_2 respectively:

$$W_{eff} = \ln\left(\frac{j_2}{j_1}\,\frac{T_1^2}{T_2^2}\right)\, k_B\, \frac{T_1 \cdot T_2}{(T_2 - T_1)} \qquad (14)$$

Implicitly, Eq. (14) assumes that A_{exp} and the Schottky effect are temperature independent. The calculation based on Eq. (14) corresponds to the graphical determination of W_e from the slope in a Richardson plot (showing $\log(j_0/T^2)$ plotted as a function of $1/T$), for example in Gu et al. (2012).

Wire, stainless steel 1.4820:											
	W_{eff} **/(eV) determined from ratio of currents at different temperatures (T_1 & T_2)**										
Sqrt Voltage $\sqrt{kV}$	**829 K & 916 K**	**829 K & 962 K**	**829 K & 1002 K**	**829 K & 1070 K**	**916 K & 962 K**	**916 K & 1002 K**	**916 K & 1070 K**	**962 K & 1002 K**	**962 K & 1070 K**	**1002 K & 1070 K**	**Average W_{eff}/eV**
1.00	2.57	2.47	2.72	2.73	2.24	2.90	2.84	3.74	3.14	2.74	2.81
1.22	2.62	2.50	2.76	2.87	2.25	2.94	3.06	3.82	3.46	3.23	2.95
1.41	2.62	2.49	2.77	2.89	2.20	2.95	3.09	3.89	3.53	3.30	2.97
1.58	2.59	2.48	2.76	2.90	2.24	2.98	3.13	3.90	3.57	3.35	2.99
1.73	2.59	2.49	2.77	2.92	2.26	2.99	3.17	3.91	3.62	3.42	3.02
1.87	2.57	2.61	2.78	2.95	2.69	3.05	3.24	3.50	3.51	3.52	3.04
2.00	2.66	2.66	2.83	3.01	2.66	3.03	3.27	3.50	3.58	3.64	3.08
2.12	2.56	2.62	2.80	3.00	2.75	3.10	3.31	3.53	3.59	3.63	3.09

Tube, stainless steel 1.4404:											
	W_e **/(eV) determined from ratio of currents at different temperatures (T_1 & T_2)**										
Sqrt Voltage $\sqrt{kV}$	**829 K & 916 K**	**829 K & 962 K**	**829 K & 1002 K**	**829 K & 1070 K**	**916 K & 962 K**	**916 K & 1002 K**	**916 K & 1070 K**	**962 K & 1002 K**	**962 K & 1070 K**	**1002 K & 1070 K**	**Average W_e/eV**
1.00	3.13	3.07	3.06	3.12	2.93	2.96	3.11	3.01	3.20	3.33	3.09
1.22	3.08	3.07	3.07	3.13	3.06	3.05	3.16	3.04	3.22	3.33	3.12
1.41	3.16	3.07	3.09	3.12	2.88	3.00	3.09	3.16	3.20	3.23	3.10
1.58	3.08	3.05	3.08	3.11	3.00	3.08	3.13	3.20	3.20	3.20	3.11
1.73	3.08	3.02	3.07	3.10	2.89	3.05	3.10	3.25	3.21	3.18	3.10
1.87	3.05	3.02	3.06	3.12	2.96	3.07	3.17	3.22	3.27	3.30	3.13
2.00	3.04	3.00	3.05	3.11	2.91	3.05	3.16	3.24	3.29	3.32	3.12
2.12	3.09	3.04	3.07	3.12	2.92	3.05	3.13	3.23	3.24	3.25	3.11

Table 2: *W_{eff} for the wire and the tube at different voltage of operation, calculated with Eq. (14), using different pairs of temperatures.*

The W_{eff} values for different combinations of temperature as a function of voltage are shown in **Table 2**. We see that the W_{eff} values show a very wide scatter. The averaged values are similar, but not identical, to the W_{eff} values calculated with the widest possible temperature interval (829 K &

1070 K). Apparently, Eq. (14) is easily affected by temperature errors, especially when T_1 and T_2 are close together. In addition, this path of evaluation is affected by deviations of the Schottky effect from the theoretically expected behaviour. This will be discussed more in detail in the following section.

5.6 Schottky Effect and Field Enhancement Factor

The theoretical magnitude of the Schottky effect depends on the electrode geometry. In case of the wire-tube arrangement, the E-field values at the wire and at the tube, E_w and E_t resp., are calculated as

$$E_w = \frac{U}{r_w \ln(\frac{r_t}{r_w})} \quad ; \quad E_t = \frac{U}{r_t \ln(\frac{r_t}{r_w})} \tag{15}$$

Here U is the voltage of operation, r_w and r_t are the wire and tube radii, resp.. As a result, the theoretical Schottky effect produces different slopes in the Schottky plots for positive polarity (with E_t, assuming TE from the tube) and negative polarity (with E_w, assuming TE from the wire). Introducing Eq. (15) into Eq. (8), we find

$$\frac{\partial \Delta W}{\partial \sqrt{U}} = e \sqrt{\frac{e}{4\pi\varepsilon_0 \, r_{t,w} \, \ln(\frac{r_t}{r_w})}} \tag{16}$$

and hence

$$\left(\frac{\partial \Delta W}{\partial \sqrt{U}}\right)_{wire} = \frac{25.7\ 10^{-3}\ eV}{\sqrt{kV}} \quad ; \left(\frac{\partial \Delta W}{\partial \sqrt{U}}\right)_{tube} = \frac{2.91\ 10^{-3}\ eV}{\sqrt{kV}} \tag{17}$$

The experimental slopes which can be observed in Figs. 5, 6 and 7 (note – the slopes are not affected by errors in the A_R^* values) are far higher than the slopes from theoretical calculation. This leads us to the conclusion that the effective E-fields at the surfaces must be much stronger compared to the theoretical values calculated from Eq. (17).

A physical explanation is found on basis of **Fig. 9**, showing the surface of a stainless steel wire after oxidation in the oven during two experimental series. We find that the surface is covered with tightly packed, sharp-edged crystals of metal oxides. This leads to a highly non-uniform distribution of the E-field on a microscopic, sub-µm level. As long as the E-field is very weak, the emission from the protruding and the sunken-in parts of the surface, resp., can be considered to be homogeneous (provided that W_e is uniform). But with increasing values of the average E-field, the emission from the protruding parts will be activated selectively due to a strong, localized increase of the Schottky effect ΔW. Meanwhile in the sunken-in parts, the emission intensity will not increase significantly, as the local field is much below the average field. In this way, with an increasing E-field, the increase of TE is more and more concentrating on the protrusions. As the emission from more and more parts of the surface falls behind compared to the emission from the protrusions, this model also predicts a decrease of the slope with an increasing E-field.

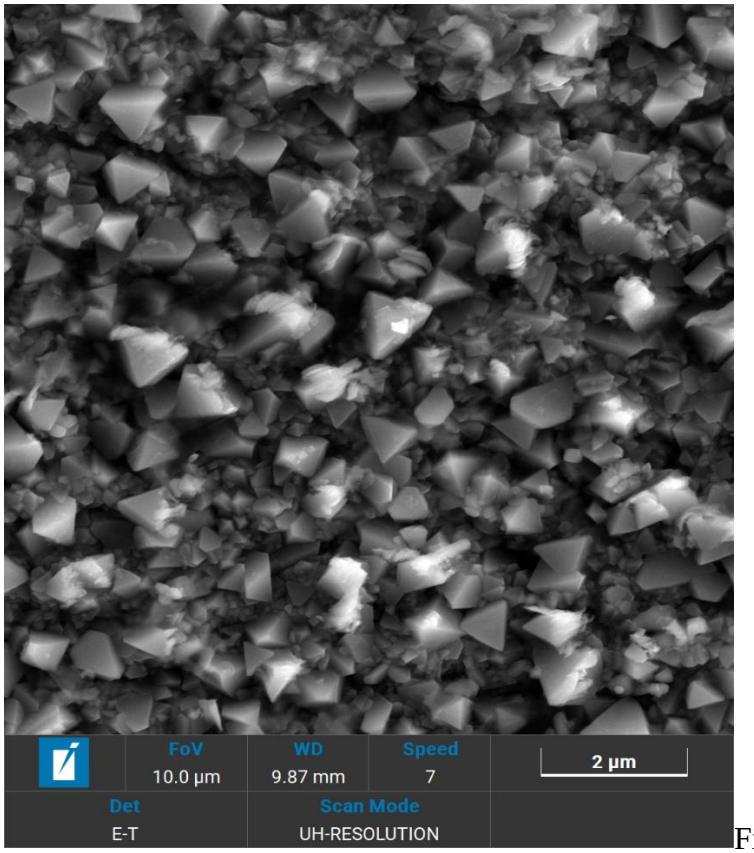

Fig.9:

Fig. 9: *SEM picture showing well-formed crystalline structures on the surface of a heat-treated stainless steel wire.*

For a quantitative description, we simplify this complicated reality rather grossly, adopting the concept of the field enhancement factor f_e from field emission. This implies that in the emission-active part of the surface, the E-field is enhanced over the average field (as calculated from Eq. (15)) by the factor f_e, while another fraction of the surface, amounting to $(1 - 1/f_e)$ for the continuity of electrostatic displacement density, is assumed to be completely inactive with respect to emission. With f_e, the empirical Schottky effect ΔW^* is written as

$$\Delta W^* = \sqrt{\frac{e^3 f_e E}{4\pi\varepsilon_0}} = \sqrt{f_e}\,\Delta W \tag{18}$$

According to the discussion given above, the f_e approach should fit better with higher surface E-fields.

Practically, f_e can be determined either by comparison between empirical and theoretical slopes in the Schottky plots, or from the ratio of TE current densities measured at equal temperature, but with different E-fields E_1 and E_2 respectively:

$$f_e = \left[\ln\left(\frac{j_2}{j_1}\right)\ \frac{k_B T}{\Delta W_{eff,2} - \Delta W_{eff,1}}\ \right]^2 \tag{19}$$

For obtaining an average of f_e, we use Eq. (19) with just two voltages which are far enough apart (1 kV & 4.5 kV), see **Table 3**. We see that significantly higher f_e values are found for emission from the tube. Either, the higher f_e values of the tube might be interpreted as a consequence of a different state of the surface, as the tube was in use much longer than the wire. Or, this effect might be explained

with the theoretical expectation discussed above, as the E-field at the tube is nearly two orders of magnitude lower compared to the E-field at the wire. Further, we also see an apparent increase of f_e with temperature, which might be explained by continuing growth of the oxide layers, as the higher temperatures were investigated later.

Voltages U_1 & U_2 (kV)	**Temperature (K)**				
	829	**916**	**962**	**1002**	**1070**
Wire (-1 & -4.5)	11.1	13.4	22.5	21.5	49.7
Tube (1 & 4.5)	227.8	236.4	253.3	377.9	370.2

Table 3: *Values of the field enhancement factor f_e determined from the ratio of currents measured at 1 kV and 4.5 kV of operation voltage, respectively.*

The E-field dependence of f_e can be confirmed when f_e is calculated for narrower voltage intervals. This is shown in **Fig. 10**, where f_e was determined for voltage intervals of 1.5 kV. Caused by inevitable measurement errors, the values of f_e scatter rather widely. Nevertheless, the data support the predicted trend of decreasing f_e with increasing voltage of operation, which is more clearly visible in case of the wire.

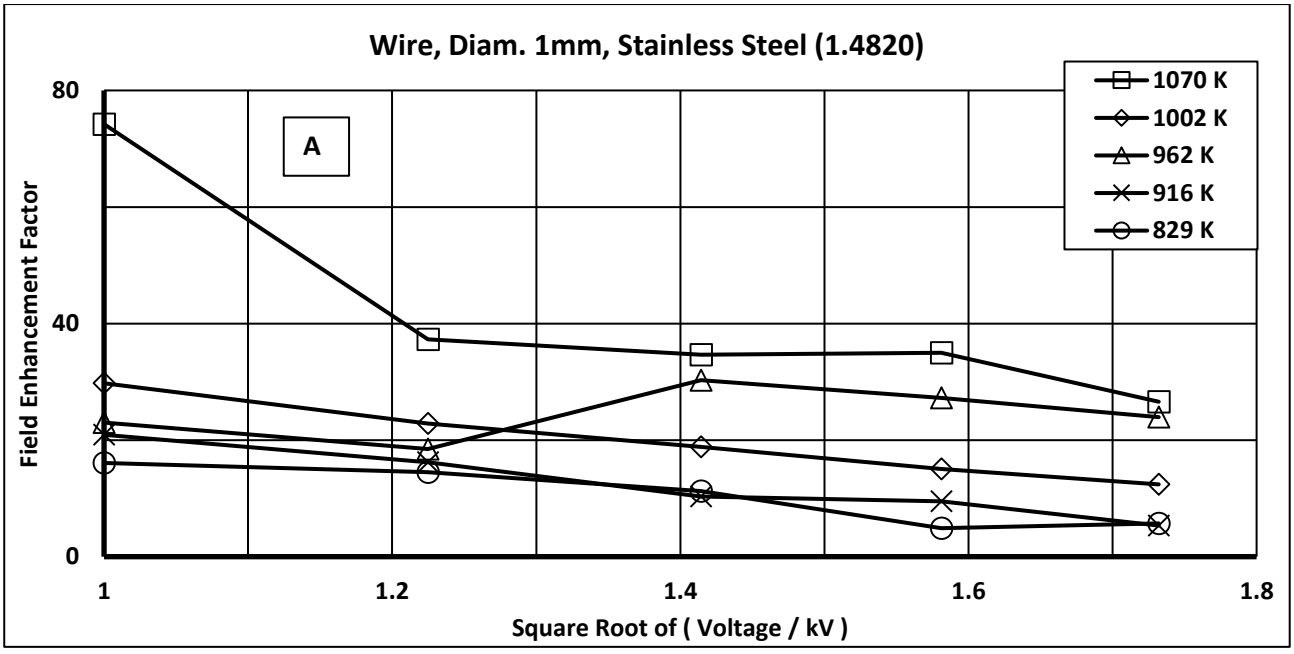

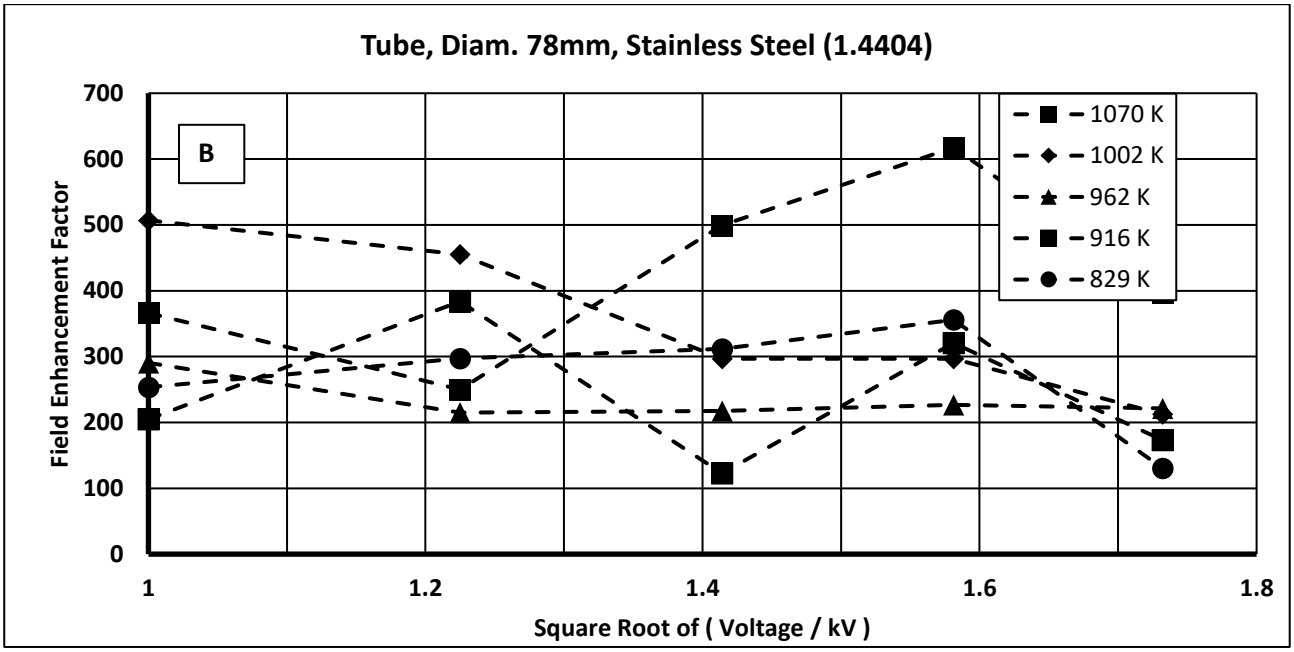

Fig. 10: *Field enhancement factors f_e calculated for the wire (**A**, above) and for the tube (**B**, below). Single points for different temperatures are calculated using the current ratio for voltage intervals of 1.5 kV. The respective f_e data points are placed in the lower end of the voltage interval.*

5.7 A Short Summary on Thermionic Emission

The thermionic emission (TE) of current in a tube – wire arrangement (tube diameter 78 mm, wire diameter 1 mm, length 860 mm) was observed and evaluated in dry air for the temperature range between 830 K and 1070 K. Using a custom-made microamperemeter installed in the high-voltage line, currents between 0.1 nA and 30 µA were measured in the voltage range below corona onset.

The emitting surfaces are of stainless steel (tube – 1.4404; wire - 1.4820). After exposure to similar temperatures during previous experiments or during a burn-in, the surfaces are covered densely with well-formed metal oxide crystals.

The evaluation of the emission data shows that the magnitude of thermionic current emission basically follows the Richardson-Schottky equation, however with a number of remarkable details:

- The Richardson constants are significantly smaller compared to the theoretical value. We found values of $6.8 \cdot 10^4 A\, m^{-2} K^{-2}$ for the wire and of $3.1 \cdot 10^4 A\, m^{-2} K^{-2}$ for the tube surface, compared to the theoretical value of $1.2 \cdot 10^6\, A\, m^{-2} K^{-2}$.
- The work function values are at 3.1 eV (wire) and 3.17 eV (tube), which is far below the vacuum values for stainless steels [Wilson 1966], [Durakievicz 2001] and also far below the vacuum values of oxidized stainless steels [Darcy & Surplice 1973].
- The Schottky effect is much stronger compared to the theoretical expectation for a smooth surface. In analogy to surface roughness effects on field emission, this can be described by the introduction of a field enhancement factor. However, a dependence of the field enhancement factor on the E-field as well as on the temperature was found experimentally. This might indicate that use of the field enhancement factor in the context of TE possibly is an oversimplification, or that an additional influence from surface oxidation is superimposed.

6 Conclusions and Future Applications

Altogether, we have been able to show that it is possible to determine the parameters of thermionic emissions by in-situ measurements on a real ESP. Our results allow to understand the role of thermionic emission for the operation of high temperature electrostatic precipitators better and in a more quantitative way. We have found that the work function of real, oxidized stainless steel surfaces is much lower than expected, which in turn explains that significant effects from thermionic emission can be observed at 700 °C already.

The current densities which were observed were quite similar for emission from the wire (at negative working electrode (WE) polarity) and from the tube (at positive WE polarity), reaching around $50\ \mu A/m$ at 800 °C. From a practitioner´s point of view, such a current density may appear insignificant. But laboratory experience with the precipitation of nanoparticle aerosols in a rather similar set-up [Bürger 2022-2] shows that in fact, extremely high separation efficiencies can be reached below corona onset at 700 °C already, with current densities in the order of $0.1\ \mu A/m$ only.

Similarly, high precipitation efficiency at very low current density was observed during aerosol precipitation in technical nitrogen with an oxygen content of 3.6 % at ambient temperature [Bürger 2020]. In these conditions, we found a free electron contribution of about 50% to the corona current. Already just above corona onset, a separation efficiency of 99.9 % was reached with a current density of 40 µA/m and a residence time of just 3 seconds.

The physics behind is that in both cases, a major part of the current transport is taken over by free electrons. At high temperature, this occurs because the oxygen anion O_2^- is not very stable and is in a temperature dependent equilibrium with the neutral oxygen molecule and the free electron:

$$O_2^- \ \Leftrightarrow\ O_2 + e^- \qquad (20)$$

With higher temperatures, the equilibrium is increasingly shifted to the right-hand side, resulting in a free-electron contribution to current transport which is growing fast with increasing temperature [Bürger 2022-1]. However, some gases such as CO_2 are able to form more stable anions (CO_4^-), which in turn reduces the fraction of free electrons.

In technical nitrogen, the formation of the free electrons (from the active corona zone) to negative ions is very slow, because the formation of the oxygen anion O_2^- requires a three-body collision between the electron and two O_2 molecules. In both cases, the high fraction of electronic current destabilizes the corona discharge and promotes sparking.

Diffusion charging by free electrons is much more efficient compared to diffusion charging by gas ions [Bürger 2020]. The background is explained as follows: Due to the large difference in mass, free electrons in an E-field are not in thermal equilibrium with the gas molecules. Instead, free electrons can accumulate a lot of energy while drifting in the passive zone of a corona discharge. The relation between the E-field and the electron energy is shown in in **Fig. 11**. At 800 °C, an E-field of 1 kV/cm corresponds to a reduced field of nearly 16 Td (1Td = 10^{-21} V·m² ≅ 0.25 kV/cm @ STP), and a free electron will accumulate a thermal energy ε of around $\varepsilon = 1\ eV$, which corresponds to an electron temperature of $T_e = 3\,\varepsilon/(2k) = 7.736\,K$. Hence, the electron temperature is about 7-fold the gas temperature. As a result, diffusion charging by free electrons will lead to a roughly 7-fold level of particle charge compared to diffusion charging by negative gas ions at comparable conditions. As

field charging is not affected by T_e, the particle size range dominated by diffusion charging will extend to significantly higher particle diameters of around 2.5 µm.

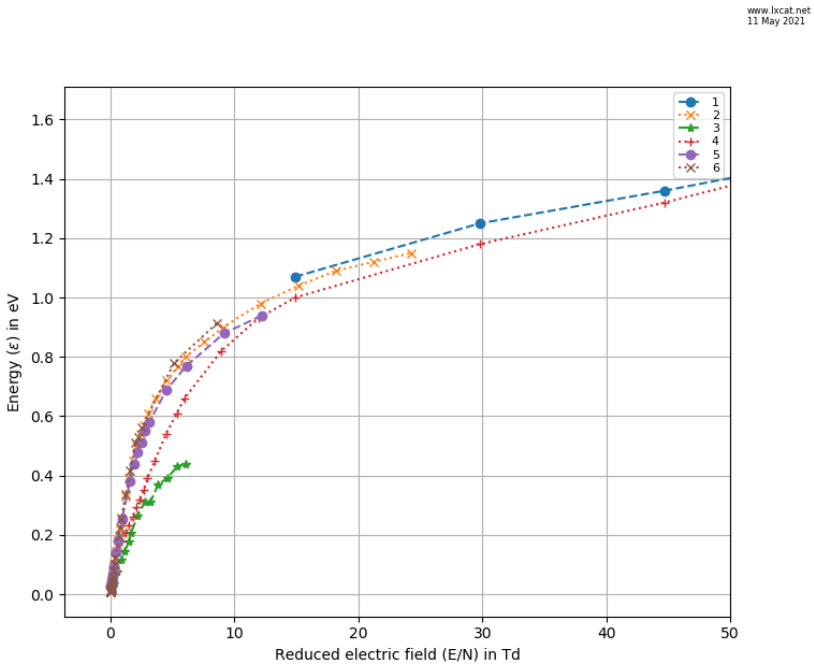

Fig. 11: *Electron energy as a function of the reduced field in nitrogen or air. Data compiled from [www.LXcat: Dutton / Heidelberg / IST Lisbon / LAPLACE databases]. For air @ STP, 10 Td ≙ 2.5 kV/cm; @ 800 °C, 10 Td ≙ 0.61 kV/cm.*

We propose to name the operation of ESPs below corona onset as the Sub-Onset Mode Of Operation (SOMOO). SOMOO offers a combination of interesting features for the range of high temperatures:

- Different from standard corona operation with negative polarity, SOMOO inherently does not produce any sparking even at the highest temperatures. As the release of charge carriers is controlled by thermionic emission, current density is distributed very uniformly.

- As far as free electrons are emitted and the E-fields are sufficiently strong, SOMOO leads to highly efficient diffusion charging with very low currents already. In the submicron and in the lower micrometer size range, SOMOO precipitation can be achieved with a very low specific input of energy.

ESPs for SOMOO operation will have to be designed differently from common ESPs. Optimum conditions for diffusion charging with thermally emitted free electrons are found with active electrodes having a rather big surface. With negative polarity and a rod electrode instead of a wire, the emissive surface is increased, the corona onset is shifted to higher voltages and a higher value of the average E-field at the precipitation electrode is possible. With positive polarity and a rod instead of a corona wire, thermionic emission will come from the tube and particle precipitation will occur onto the rod. This opens up new possibilities of electrode cleaning or possibly, of electrode exchange instead of cleaning.

The practical applicability of ESPs operating with thermionic emission in the sub-onset mode is not yet fully clear. Preliminary experiments with aerosols in the submicron range are extremely

encouraging. Analogous situations in the industry are found, for example, in case of the post-combustion of gases containing VOCs with admixture of silicon compounds.

On the other hand, some of the references show that positive ions, notably alkali metal ions such as Na^+ and K^+, have comparably low or even lower values of the work function compared to free electrons and might be emitted when they are present in the process. The emission of positive ions from the precipitation electrode would create a bipolar situation and might lead to a serious deterioration of the precipitation efficiency.

Therefore, much more experience will be needed to understand the full potential of high temperature ESPs for a wider range of applications. More work should be devoted to study thermionic emission from different high temperature materials in combination with the effects from different temperature-time histories. Equally important will be to gain knowledge about thermionic emission from dust-covered surfaces. And finally, thermionic emission from the aerosol particles themselves has to be included. Other than at lower temperatures, particle charging at high temperature is not a one-way process.

The authors are convinced that high temperature ESPs will be an important part of future energy efficient production processes in the industry, as they pave the way for efficient high temperature heat recovery. Therefore, it is worth to take a big effort for the development of this key technology.

References:

Bürger P., Riebel U. (2020:) Electrostatic charging and precipitation of nanoparticles in technical nitrogen: Highly efficient diffusion charging by hot free electrons. Journal of Aerosol Science, 141, 105495.

Bürger P., Riebel U. (2022-1): High temperature coronas in air and flue gas from LPG combustion: Current-voltage characteristics, ion mobilities and free electrons. Journal of Electrostatics, 115, 103676.

Bürger, P., Riebel, U. (2022-2): Feasibility of high-temperature electrostatic precipitation for the removal of nanoparticles: A case study on iron oxide separation at up to 800 °C, FILTECH 2022 Conference Proceedings, Session G5, Cologne, Germany, ISBN: 978-3-941655-19-5.

Christensen J.M., Grunwaldt J.-D., Anker D. J. (2016): Importance of the oxygen bond strength for catalytic activity in soot oxidation. Applied Catalysis B: Environmental 188, pp. 235–244

D´Arcy R.J., Surplice N.A. (1973): Electric charges on stainless steel surfaces: The effects of hydrogen, charged particles, illumination, and electric fields on the work function. Surface Sci. 34 (2), 193 - 211.

Durakiewicz T., Arko A.J., Joyce J.J., Moore D.P., Halas S. (2001): Thermal work function shifts for polycrystalline metal surfaces. Surface Science 478, 72 - 82.

Fujiwara Y., Sakai T., Kaimai A., et al. (2006): Continuous emission of ions into a vacuum from a bare surface of yttria stabilized zirconia at elevated temperatures. J. Vac. Sci. Technol. A 24, 1818.

Gu Z., Xi X., Yang J., Xu J. (2012) Properties of RE–W cathode and its application in electrostatic precipitation for high temperature gas clean-up. Fuel, 95, pp. 648–654.

Hagström M., Jäglid U., Pettersson J.B.C. (2000): Desorption kinetics at atmospheric pressure: alkali interactions with rhodium and steel surfaces. Applied Surface Science 161, pp. 291–299.

Jenkins R. O. (1969): A review of thermionic cathodes. Vacuum 19 (8) pp. 353-359.

Lampert M. A. (1956): Simplified theory of space-charge-limited currents in an insulator with traps, Phys. Rev. 103 1648.

Nishioka M., Torimoto Y., Kashiwagi H., Li Q., Sadakata M. (2003): Features and mechanism of atomic oxygen radical anion emission from yttria-stabilized zirconia electrolyte. J. of Catalysis 215 pp. 1–6.

Parker K.R. (ed) (1997) Applied electrostatic precipitation, 1st Ed. Springer Netherlands, Dordrecht.

Peek F.W. (1920) Dielectric phenomena in high voltage engineering, 2nd Ed. McGraw Hill, London, New York

Raizer Y.P. (1991) Gas discharge physics. Springer-Verlag, Berlin Heidelberg

Richardson O.W. (1929): Thermionic phenomena and the laws which govern them. Nobel Lecture.

Rietwyk K.J., Keller D.A., Ginsburg A. et al (2019): Universal work function of metal oxides exposed to air. Adv. Mater. Interfaces 2019, 6, 1802058.

Rinard G., Rugg D.E., Yamamoto T. (1987) High-Temperature High-Pressure Electrostatic Precipitator Electrical Characterization and Collection Efficiency. IEEE Transactions on Industry Applications, IA-23, pp. 114–119.

Serdyuk Y. V., Gubanski S. M. (2005): Computer modelling of interaction of gas discharge plasma with solid dielectric barriers, IEEE Transactions on Dielectrics and Electrical Insulation, 12 (4)

Skinner S.J., Kilner J.A. (2003): Oxygen anion conductors. Materials Today, 2003 (3), pp. 30 – 37.

Ura B., Trawczynski J., Kotarba A., et al. (2011): Effect of potassium addition on catalytic activity of SrTiO3 catalyst for diesel soot combustion. Applied Catalysis B: Environmental 101, pp. 169–175.

Weber E., Wiggers H., Morgenstern U. (1993) Erprobung eines Plattenelektrofilters fuer die Erprobung eines Plattenelektrofilters für die Hochtemperatur-Hochdruck-Entstaubung unter Berücksichtigung spezieller Effekte. Luft und Kältetechnik, 4, pp. 165–168.

White H.J. (1963) Industrial Electrostatic Precipitation. Addison-Wesley Publishing Company, Inc., Reading, Mass.

Wilson R.G. (1966): Vacuum thermionic work functions of polycrystalline Be, Ti, Cr, Fe, Ni, Cu, Pt, and type 304 stainless steel. J. of Applied Physics 37, 2261-2267.

Yamazaki K., Sakakibara Y., Dong F., Shinjoh H. (2014): The remote oxidation of soot separated by ash deposits via silver–ceria composite catalysts. Applied Catalysis A: General 476, pp. 113–120.

Zeng L., Weber A.P. (2012): Transportmechanismen für aktivierten Sauerstoff in der katalytischen Rußoxidation an Nanopartikel-Schichtsystemen. Chemie Ingenieur Technik 84 (3), pp. 295–300.